LIMNOLOGY and OCEANOGRAPHY

ASLO

Limnol. Oceanogr. 66, 2021, 108–122

doi: 10.1002/lno.11591

Seasonal microbial food web dynamics in contrasting Southern Ocean productivity regimes

Urania Christaki,[1]* Audrey Gueneugues,[2] Yan Liu,[2] Stéphane Blain,[2] Philippe Catala,[2] Jonathan Colombet,[3] Pavla Debeljak,[2] Ludwig Jardillier,[4] Solène Irion,[1] Fred Planchon,[5] Ingrid Sassenhagen,[1] Telesphore Sime-Ngando,[3] Ingrid Obernosterer[2]

[1]Univ. Littoral Côte d'Opale ULCO, CNRS, Univ. Lille, UMR 8187, LOG, Laboratoire d'Océanologie et de Géosciences, F-Code postal Ville, France

[2]Sorbonne Université, CNRS, Laboratoire d'Océanographie Microbienne (LOMIC), Banyuls-sur-Mer, France

[3]Laboratoire Microorganismes: Génome et Environnement (LMGE), UMR CNRS 6023, Clermont Université Blaise Pascal, Aubière Cedex, France

[4]Unité d'Ecologie, Systématique et Evolution, Université Paris-Sud, CNRS, AgroParisTech, Université Paris-Saclay, Orsay Cedex, France

[5]University of Brest, Laboratoire des Sciences de l'Environnement (LEMAR), UMR6539 CNRS/UBO/IFREMER/IRD, Technopôle Brest Iroise, Plouzané, France

Abstract

Spatial and seasonal dynamics of microbial loop fluxes were investigated in contrasting productivity regimes in the Indian sector of the Southern Ocean. Observations carried out in late summer (February–March 2018; project MOBYDICK) revealed higher microbial biomasses and fluxes in the naturally iron-fertilized surface waters of Kerguelen island in comparison to surrounding off-plateau waters. Differences were most pronounced for bacterial heterotrophic production (2.3-fold), the abundance of heterotrophic nanoflagellates (HNF; 2.7-fold). Independent of site, grazing by HNF was the main loss process of bacterial production (80–100%), while virus-induced mortality was low (< 9%). Combining these results with observations from previous investigations during early spring and summer allowed us to describe seasonal patterns in microbial food web fluxes and to compare these to carbon export in the iron-fertilized and high-nutrient, low-chlorophyll (HNLC) Southern Ocean. Our data suggest an overall less efficient microbial food web during spring and summer, when respiration and viral lysis, respectively, represent important loss terms of bacterially-mediated carbon. In late summer, primary production is more efficiently transferred to bacterial biomass and HNF and thus available for higher trophic levels. These results provide a new insight into the seasonal variability and the quantitative importance of microbial food web processes for the fate of primary production in the Southern Ocean.

The Southern Ocean plays a major role in the global carbon cycle, yet there are still major gaps in our understanding of how it fully functions (e.g., Gruber et al. 2009; Gray et al. 2018). Investigations into biogenic C-export in the Southern Ocean suggest an inverse relationship between primary production and carbon export efficiency (Lam and Bishop 2007; Maiti et al. 2013; LeMoigne et al. 2016). Differences in phytoplankton community composition may affect trophic structure, grazing intensity and/or microbial remineralization (e.g., Maiti et al. 2013; LeMoigne et al. 2016). At present, no model can reasonably calculate carbon export in the Southern Ocean, partly because, neither primary production nor food web structure can predict these fluxes (Rembauville et al. 2015; LeMoigne et al. 2016; Deppeler and Davidson 2017). Observational studies of planktonic communities and their activities in this remote ocean can thus offer essential information in understanding the current and future state of the mechanisms that link planktonic communities with carbon export (Rembauville et al. 2015).

The Southern Ocean is the largest high-nutrient, low-chlorophyll (HNLC) zone where the limitation of primary production by iron is spatially heterogeneous (Blain et al. 2007). In this context, the contrasting iron-fertilized and HNLC areas

*Correspondence: urania.christaki@univ-littoral.fr

Additional Supporting Information may be found in the online version of this article.

Urania Christaki and Ingrid Obernosterer have equal contribution.

[Corrections updated on Sep 24, 2020, after first online publication]

around the Kerguelen and Crozet islands provide an excellent environment to investigate the spatial and temporal heterogeneity of planktonic C-fluxes in the Southern Ocean (Blain et al. 2007; Pollard et al. 2007, 2009). The extensive phytoplankton blooms occurring in iron-fertilized waters, mainly characterized by diatom communities (e.g., Poulton et al. 2007; Lasbleiz et al. 2016), have higher primary production rates (Seeyave et al. 2007; Cavagna et al. 2015) and higher carbon export in contrast to the surrounding HNLC waters (Savoye et al. 2008; Planchon et al. 2015). The Kerguelen bloom, -despite being a major carbon sink with high CO_2 sequestration per unit of iron (Blain et al. 2007), follows the "High Biomass Low Export" paradigm (Lam and Bishop 2007) of the Southern Ocean (Mosseri et al. 2008; Savoye et al. 2008; Cavagna et al. 2015; Planchon et al. 2015).

Microbial food web processes determine to a large extent what fraction of primary production is remineralized or available for higher trophic levels or export. The fraction of primary production consumed by heterotrophic bacteria is highly variable in polar oceans (Kirchman et al. 2009), likely resulting from variable degrees of phytoplankton-bacteria coupling (Morán et al. 2006). In Kerguelen plateau waters, heterotrophic bacteria respond rapidly to the phytoplankton bloom and process a considerable fraction of the primary production (Obernosterer et al. 2008; Christaki et al. 2014). Protists channel prokaryotic carbon to higher trophic levels through bacterivory while viruses return dissolved and small particulate prokaryotic carbon forms to the water column via the viral shunt. Theoretically, grazing should therefore enhance carbon export while viral lysis would enhance respiration and reduce prokaryote growth efficiency. Viral activity in the Southern Ocean could be crucial for iron regeneration, especially in HNLC areas (Strzepek et al. 2005; Evans and Brussaard 2012). This said, integrative studies of microbial stocks (viruses, heterotrophic bacteria, heterotrophic and phototrophic flagellates) and fluxes (bacterial production, respiration, grazing and viral lysis) along with community production and C-export measurements are necessary to describe the role of bacteria in C-flux variability.

The present study was undertaken in the framework of the MOBYDICK project (Marine Ecosystem Biodiversity and Dynamics of Carbon around Kerguelen: an integrated view). MOBYDICK's objective was to trace C from its biological fixation, cycling within and across trophic levels, and its export to depth, under different productivity regimes of the Southern Ocean in late summer. Our aim here was to compare C-fluxes mediated by microbes at the surface to carbon export to deeper layers and carbon availability for higher trophic levels at the surface. Seasonal dynamics of bacterial carbon processing in iron-fertilized and HNLC waters and its implications for ecosystem functioning is described during three periods, separated by 7 to 13 yr: early spring (onset of the bloom, October–November 2011, KEOPS2 cruise), summer (decline of the bloom, January–February 2005, KEOPS1 cruise 2005), and end of summer (post-bloom period, February–March 2018, MOBYDICK cruise).

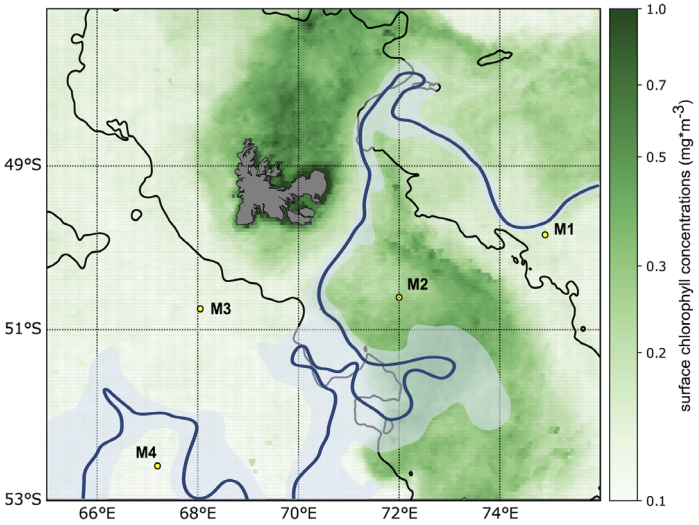

Fig 1. Map of the MOBYDICK station locations. Surface chlorophyll *a* (Chl *a*) concentrations were Reprocessed Global Ocean Satellite Observations (Copernicus-GlobColour). Data were provided by Copernicus Marine Service (http://marine.copernicus.eu/). Chl *a* concentrations are the monthly means for March 2018 at a resolution of 4 km. The black lines denote 1000 m bathymetry. The approximate position of the highly dynamic polar front during February-March 2018 was also drawn according to Pauthenet et al. (2018). The polar front is the dark, thick, blue line, gray zone around the polar front indicates variations in its trajectory.

Materials and methods

Sample collection

Samples were collected at four stations (M1, M2, M3, and M4) in the region of Kerguelen island in the Indian sector of the Southern Ocean during late austral summer (19 February to 20 March 2018; MOBYDICK cruise) (Fig. 1). The timing of the visits corresponded to about one month after the seasonal maximum in chlorophyll *a* (Chl *a*) (Figs. S1, S2). Sta. M2 was located above the Kerguelen plateau and is the "historical" A3 station of the previous KEOPS1 and KEOS2 cruises (Figs. 1, S1). This site is located in naturally iron-fertilized waters and characterized by high primary production during spring and summer (Lefèvre et al. 2008; Mosseri et al. 2008; Cavagna et al. 2015). Sta. M1, M3, and M4 were located off the plateau characterized by lower seasonal primary production (Fig. S1). Sta. M2 was sampled three times with an eight day interval between visits (M2-1, M2-2, M2-3; Table 1). Sta. M3 (M3-1, M3-3) and M4 (M4-1, M4-2) were both sampled twice with a 2-week interval each, and Sta. M1 was visited once (Table 1). All water samples were collected with 12L Niskin bottles mounted on a rosette equipped with CTD (SeaBird 911-plus). Microbial parameters were sampled at selected depths throughout the water column (Table 2).

Viral and microbial abundance

Pico- and nanophytoplankton, virus-like particles, heterotrophic bacteria (sensus-stricto includes *Archaea* and *Bacteria*), and heterotrophic nanoflagellates (HNF) were enumerated

Table 1. Station description. The depth of the mixed layer (Z_{ML}) is based on a difference in sigma of 0.02 to the surface value. The mean Z_{ML} and euphotic layer (Ze = 1% light depth) of all CTD casts performed during the occupation of the stations is given. For the rest of the variables the mean ± SD is given for the mixed layer.

Sta.	Date (2018)	Long (°E)*	Lat (°S)*	Depth (m)*	Z_{ML} (m)	Z_e (m)	T (°C)	Chlorophyll *a* ($\mu g\ L^{-1}$)	$NO_3^- + NO_2^-$ (μM)	NH_4^+ (μM)	PO_4^{3-} (μM)	Si $(OH)_4$ (nM)
M2-1	26–28 Feb	72.0004	50.3697	520	62	64	5.10 ± 0.06	0.27 ± 0.02	21.9 ± 0.12	0.75 ± 0.07	1.47 ± 0.03	1.36 ± 0.41
M2-2	6–8 Mar	72.0099	50.3769	519	61	61	5.24 ± 0.00	0.30 ± 0.04	21.79 ± 0.38	1.12 ± 0.02	1.50 ± 0.04	1.72 ± 0.79
M2-3	16–17 Mar	72.0013	50.3700	527	68	58	5.11 ± 0.07	0.58 ± 0.02	21.9 ± 0.08	0.95 ± 0.05	1.50 ± 0.00	2.75 ± 0.27
M1	8–9 Mar	74.5406	49.5098	2723	27	80	4.99 ± 0.10	0.35 ± 0.040	25.2 ± 0.56	0.56 ± 0.20	1.71 ± 0.11	8.38 ± 2.93
M3-1	3–5 Mar	68.0347	50.4095	1000	65	93	5.6 ± 0.00	0.20 ± 0.02	23.75 ± 0.31	0.50 ± 0.03	1.65 ± 0.05	2.89 ± 1.01
M3-3	18–20 Mar	68.0302	50.4193	1700	79	107	5.31 ± 0.02	0.14 ± 0.00	23.34 ± 0.12	0.73 ± 0.01	1.08 ± 0.92	2.31 ± 0.04
M4-1	28 Feb–3 Mar	67.1198	52.3601	4186	49	96	4.45 ± 0.06	0.18 ± 0.01	25.7 ± 0.05	0.37 ± 0.03	1.70 ± 0.02	4.36 ± 0.35
M4-2	12–14 Mar	67.1228	52.3610	4300	87	100	4.46 ± 0.00	0.21 ± 0.00	24.8 ± 0.27	0.48 ± 0.01	1.71 ± 0.01	4.80 ± 0.00

* Coordinates and depth of the CTD "stock."

from surface to 450–1000 m. Samples for virus-like particles and heterotrophic bacteria (2.5 mL) were fixed with 1% v/v glutaraldehyde. Samples for HNF were fixed with 1% v/v paraformaldehyde prepared on board. Samples were stored at 4°C for 40 min, flash frozen in liquid nitrogen and then kept at −80°C until analysis. Counts for heterotrophic bacteria were made after staining with SYBRGreen I by flow cytometric analysis on a BD FACS Canto. Two heterotrophic bacteria populations were discriminated, one with high fluorescence called "high nucleic acid" and one with low fluorescence called "low nucleic acid". Pico-nanophytoplankton and cyanobacteria of the genus *Synechococcus* were discriminated based on their side scatter and red fluorescence. HNF and virus-like particles were enumerated after staining with SYBRGreen I on a Cytoflex Beckman-Coulter flow cytometer, following Christaki et al. (2011) and Brussaard (2004), respectively. As for bacteria, two populations of virus-like particles could be distinguished based on their fluorescence intensity. Ciliates and dinoflagellates were counted in acid Lugol's (2% v/v) fixed samples (500 mL) under an inverted microscope (Nikon Eclipse TE2000-S ×400).

Bacterial production

Heterotrophic bacterial production was measured from surface to 500 m with the ^{3}H-leucine incorporation method. At each depth 20 mL triplicate samples and a formalin killed control (2% v/v) were spiked with a mixture of nonradioactive (19 nM) and L-[4.5-^{3}H] leucine (Perkin Elmer,120 Ci/mmol). The concentration of radioactive leucine was 1 nM in the mixed layer and 2 nM below the mixed layer. Concentration kinetics were checked at 25 and 250 m with 4, 6, 12, 20, and 40 nM of leucine, to ensure that there was no isotopic dilution. The incubation times were 2 h in the 0–150 m layer, 4 h in the 150–200 m layer, and 8 h in the 250–500 m layer. Time kinetics were tested for 10, 125, 250, and 500 m (0, 3, 6, 8, 10 h) and were found linear for the applied incubation times. Samples were incubated in the dark at in situ temperature. Incubations were terminated with formalin (2% v/v). Samples were filtered onto 0.22 μm Nuclepore filters, after filtration ice-cold 5% trichloroacetic acid (10 mL) was added on the filters for 10 min. The filters were rinsed 3 times with 4 mL ice-cold 5% trichloroacetic acid, placed in scintillation vials where 8 mL of scintillation cocktail (Ultima Gold—Packard) was added and radioassayed on board. Incorporation rates of leucine into carbon were calculated using a theoretical conversion factor of 1.55 kg of C mol^{-1} (Kirchman 1993).

Dark community and bacterial respiration, net community production, and gross community production

Rates of dark community respiration, bacterial respiration and net community production were determined from changes in the concentration of dissolved oxygen (O_2) during 24 h light and dark incubations as described previously (Lefèvre et al. 2008). For dark community respiration and net

Table 2. Parameters sampled. Virus-like particles (VLP), heterotrophic bacteria (HB), heterotrophic nanoflagellates (HNF), phototrophic pico- and nanoplankton (PNP), bacterial heterotrophic production (BP), bacterial respiration (BR), gross community production (GCP), dark community respiration (DCR), net community production (NCP), virus induced bacterial mortality (VIBM), grazing induced bacterial mortality (GIBM), photosynthetically active radiation (PAR).

Parameter	Sta.	Depth (m)
VLP, HB, HNF, PNP	All	10,15 or 20, 30, 50, 60, 70, 100, 125, 150, 175, 200, 350, 450, 500 (except M2, 450 m)
BP	All	Same as above
BR	All, except M3-1	50%, 1% PAR level
GCP, DCR, NCP	All, except M3-3	50%, 25%, 4%, 1% PAR level
VIBM	All	10, 60, 125, 300 m
GIBM	All, except M3-3, M4-2	30 m

community production, seawater was collected at four depths corresponding to 1%, 4%, 25%, and 50% of photosynthetically active radiation levels of surface values. Unfiltered seawater was transferred to 125 mL borosilicate glass bottles and incubated in an on-deck incubator at the respective photosynthetically active radiation levels using optical density filters (Nickel screens). The outdoor incubators were connected with a running seawater system to maintain the incubation bottles at the temperature of the mixed layer zone. The 1% light depth (euphotic depth) was at the bottom of the mixed layer at Sta. M2, but the euphotic depth was well below the mixed layer at the off-plateau sites (Table 1). Gross community production was calculated as the sum of dark community respiration and net community production. For bacterial respiration, seawater from two depths corresponding to the 1% and 50% surface photosynthetically active radiation levels were filtered through 0.8 μm polycarbonate filters (Nuclepore) and the subsequent filtrate was incubated in 125 mL borosilicate bottles in the dark at in situ temperature for 1–3 days (Obernosterer et al. 2008). All incubations were done in five replicates. Dissolved oxygen (O_2) concentration was determined by spectrophotometric detection of iodine following the Winkler reaction, using a Hitachi U-3010 Spectrophotometer equipped with a sipper system.

Grazing induced bacterial mortality

Bacterial mortality due to protists was evaluated in the mixed layer (30 m) using the principle of fluorescently labeled bacteria (FLB) as prey analogues (Sherr et al. 1987). The FLB were prepared with a culture of *Brevundimonas diminuta* (CECT 313) following the protocol of Sherr et al. (1987). Triplicate glass Schott bottles of 2 L were filled with 60 μm screened water directly from the Niskin bottle and one control with 0.2 μm filtered sea water were inoculated with FLB at a final concentration of approx. 0.7×10^5 mL^{-1} in a refrigerated room (4°C). The expected FLB to bacteria ratio-based on bacterial abundances during previous cruises was expected to be around 20%. Because of increased bacteria abundances during MOBYDICK, this ratio was of 6–14%. After addition of labeled preys in all bottles, samples for FLB, heterotrophic bacteria and HNF counts were immediately withdrawn for T_0 counts. Incubations were performed in an on-deck incubator with surface seawater circulation, covered with a screen providing 50% light attenuation. Grazing on bacteria was measured by counting both the number of ingested FLB in food vacuoles by microscopy and FLB disappearing by flow cytometry. The food vacuole observation approach allows visual observation of the proportion and the morphology of protists that ingested FLB. Both approaches are based on several assumptions which will be further discussed in the paper.

Food vacuole analysis

After 4 h of incubation, 45 mL samples were retrieved from the bottles, fixed with glutaraldehyde (1% final conc.) and filtered on 0.8 μm Nuclepore filters before being stained with DAPI (4′,6-diamidino-2-phenylindole). They were then kept frozen at −80°C until they were observed with a Zeiss AX10 epifluorescence microscope. Prokaryotes were identified by their blue fluorescence when excited with UV radiation, while DTAF (4,6-dichlorotriazinyl-aminofluorescein) stained FLB were identified by their yellow-green fluorescence when excited with blue light. The ingestion rate (IR: FLB HNF^{-1} h^{-1}) was calculated according to Dolan and Šimek (1998) as:

$$\mathrm{IR} = \mathrm{VC} \times k, \quad (1)$$

where VC is vacuole content at steady state, and k is a conservative digestion rate of 0.92% cell content min^{-1}, which corresponds to a $t_{1/2}$ digestion time of 75 min. For comparison, a higher k of 1.1% was also calculated ($t_{1/2}$ digestion time of 63 min).

Fluorescently labeled bacteria disappearance

Bottles were incubated for approximately 50 h. Samples for procaryotes, FLB, and HNF abundances were taken every 10–12 h. Samples were fixed and stored for flow cytometry as

described above. Triplicate counts by flow cytometry were performed for each sample. Bacterial grazing rates were obtained by measuring the rate of disappearance of FLB after subtracting the FLB disappearance in the "control." The abundance of FLB was plotted vs. time, and the calculation of grazing rates (g, h^{-1}) of FLB corresponds to the slope of the abundance of FLB as a function of time. The decrease of FLB abundance was linear for the first 40–48 h, at the exception of M2-3 where it was linear only for the first 24 h. The "control" bottles showed no decrease of FLB during the incubations. In the experimental bottles, the abundances of bacteria and nanophytoplankton did not show significant increases or decreases for the first 40 h. The impact of protists on bacteria was calculated as the % of the bacterial production consumed, assuming that FLB were grazed at the same rates as natural bacteria (Sherr et al. 1987).

For comparison with FLB disappearance and vacuole content analysis, the potential consumption of bacteria by HNF and ciliates was also estimated assuming a clearance rate of 10^5 cell volume h^{-1} (Fenchel 1982). For all approaches, the % of bacterial production consumed was calculated from the number of bacterial cells produced as determined by leucine incorporation (see above).

Virus-induced bacterial mortality

Triplicate 4.5 mL samples, collected at each depth (Table 2), were fixed and stored as for flow cytometry (see above). Upon analysis, they were pooled and ultracentrifugated in order to harvest the bacterial cells for transmission electron microscope observations (detailed in Christaki et al. 2014). Virus induced bacterial mortality (VIBM) was calculated as (Eq. 2, Binder 1999; Eq. 3, Weinbauer et al. 2002):

$$\mathrm{VIBM} = \left(\mathrm{FIC} + 0.6 \times \mathrm{FIC}^2\right) / (1 - 1.2 \times \mathrm{FIC}) \quad (2)$$

$$\mathrm{FIC} = 9.524 \times \mathrm{FVIC} - 3.256 \quad (3)$$

where FIC is the frequency of infected cells, and FVIC is the frequency of visibly infected cells (i.e., cells that contain five or more phages).

Statistical analyses

Principal component analysis (PCA) and hierarchical clustering on principle components was performed on environmental variables with *R*-software, version 3.5.1 using the package FactoMineR (Lê et al. 2008). Before these analyses, environmental variables were standardized to zero mean using function "decostand" in the package vegan (Oksanen 2017).

Results

Environmental context

The hydrological context of the stations was characterized by the location of the polar front during the MOBYDICK

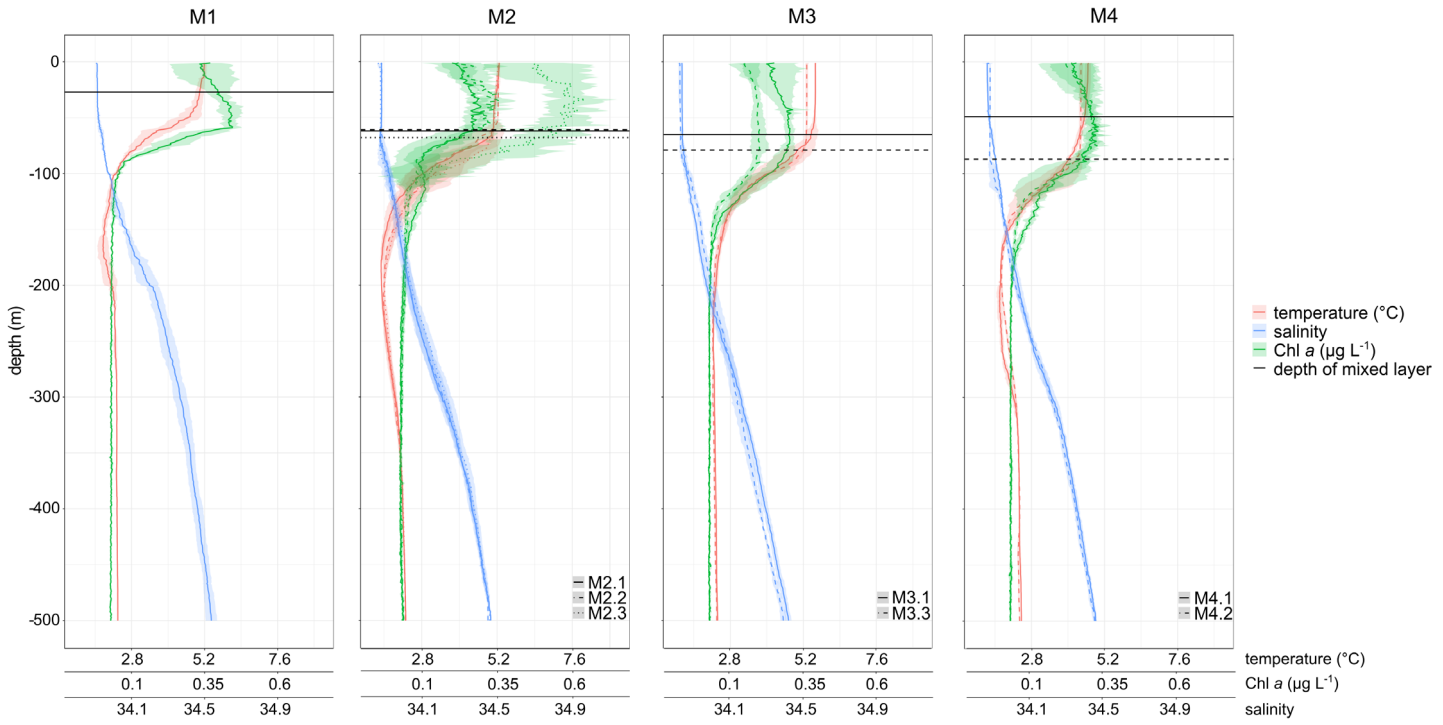

Fig 2. Temperature (°C), salinity and chlorophyll *a* (Chl *a*) (derived from in vivo fluorescence) profiles for all the visits at the four stations. The mean profiles were calculated from all the CTDs of each visit to a station, the shadows around the mean profiles are standard deviations.

cruise. Sta. M1, situated in Antarctic waters, was influenced by the highly dynamic polar front (Pauthenet et al. 2018), resulting in a shallow mixed layer (27 m, Table 1, Figs. 1, 2). Sta. M2 and M4 were located south of the polar front in Antarctic waters with a characteristic temperature minimum zone close to 200 m (Figs. 1, 2) and a mixed layer varying between 61–68 m, and 49–87 m, respectively (Table 1, Fig. 2). Sta. M3 was situated in the sub-Antarctic zone outside the influence of the polar front (mixed layer depth, 65–79 m). Temperature in the mixed layer was lowest at Sta. M4 (4.5°C) and highest at Sta. M3 (5.6°C, Table 1). The mixed layer deepened at all stations after a storm that occurred on the 10th of March 2018. The greatest increase in the mixed layer depth induced by the storm was observed at Sta. M4 (77%, from 49 to 87 m) while at stations M2 and M3 the increase of the mixed layer depth was moderate (10% and 20%, respectively, Table 1).

Average Chl *a* concentrations in the mixed layer ranged from 0.14 (M3-3) to 0.58 μg L^{-1} (Sta. M2-3). Chl *a* in the mixed layer doubled from the first to the third visit at Sta. M2 3 weeks later (from 0.27 to 0.58 μg L^{-1} Table 1, Fig. 2). Phosphate and nitrate were abundant in the mixed layer at all stations, while the highest ammonium concentrations were observed on the plateau at Sta. M2 (0.75–1.12 μM). Silicic acid concentration was overall higher off the plateau (2.3–8.4 μM) than in surface waters on the Kerguelen plateau (1.4–2.8 μM, Table 1). The first two components of the principal

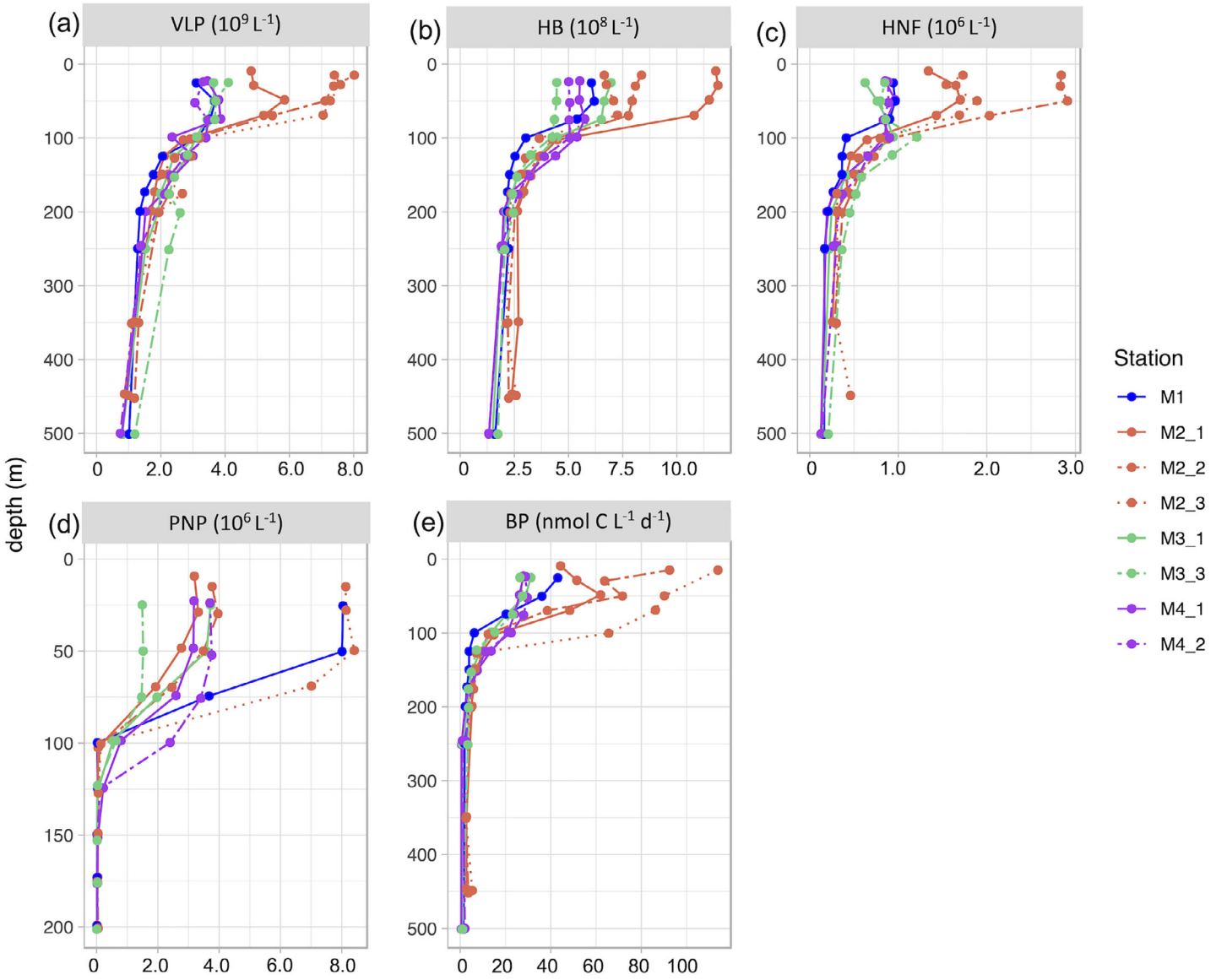

Fig 3. Vertical profiles of viral-like particles (VLP) (**a**), heterotrophic bacteria (HB) (**b**), heterotrophic nanoflagellates (HNF) (**c**), phototrophic pico- and nanoplankton (PNP) (**d**), and bacterial production (BP) (**e**).

Table 3. Mean ± SD values of all visits at the M2 plateau station and the off-plateau stations (M1, M3, and M4). heterotrophic bacteria (HB), % of high and low DNA bacteria as defined by flow cytometry (%"high nucleic acid", %"low nucleic acid"), virus like particles (VLP), % of low and high green fluorescence VLP (VLP1 VLP2), heterotrophic nanoflagellates (HNF), pico- and nanophytoplankton (PNP) and *Synechococcus* spp. at on-plateau (M2) and the off-plateau stations (M1, M3, M4).

	HB (10^8 L^{-1})		HB "high nucleic acid" %		HB "low nucleic acid" %	
Layer	**M2**	**Off plateau**	**M2**	**Off plateau**	**M2**	**Off plateau**
Mixed layer (Z_{ML})	8.8 ± 2.1	5.3 ± 1.1	56 ± 2	41 ± 3	44 ± 4	59 ± 3
Z_{ML}–200 m	4.1 ± 2.3	3.1 ± 1.0	57 ± 2	52 ± 4	43 ± 4	58 ± 4
200–500 m	2.4 ± 0.2	1.5 ± 0.6	52 ± 5	46 ± 2	46 ± 3	54 ± 2
	VLP (10^9 L^{-1})		**%VLP1**		**%VLP2**	
Layer	**M2**	**Off plateau**	**M2**	**Off plateau**	**M2**	**Off plateau**
Mixed layer (Z_{ML})	6.46 ± 0.9	3.35 ± 0.07	90 ± 1	89 ± 3	10 ± 1	11 ± 3
Z_{ML}–200 m	2.41 ± 0.05	2.26 ± 0.06	86 ± 3	85 ± 2	14 ± 3	15 ± 2
200–500 m	1.17 ± 0.05	1.24 ± 0.04	86 ± 6	84 ± 2	14 ± 6	16 ± 2
	HNF (10^6 L^{-1})		**PNP (10^6 L^{-1})**		***Synechococcus* (10^3 L^{-1})**	
Layer	**M2**	**Off plateau**	**M2**	**Off plateau**	**M2**	**Off plateau**
Mixed layer (Z_{ML})	1.96 ± 0.5	0.83 ± 0.13	4.71 ± 1.9	3.33 ± 2.1	73 ± 16	111 ± 88
Z_{ML}–200 m	0.51 ± 0.1	0.53 ± 0.27	0.52 ± 0.31	0.22 ± 0.52	10 ± 5	12 ± 16
200–500 m	0.25 ± 0.08	0.19 ± 0.08	–	–	–	–

component analysis (PCA) of environmental parameters in the mixed layer explained 76% of the variability of the data (Fig. S3). Phosphate, nitrate and ammonium were the most important variables for the principal component axis formation. Sta. M2 was associated with higher ammonium concentrations while Sta. M4 presented the highest nitrate, phosphate and silicic acid concentrations, and Sta. M1 was associated to high dissolved oxygen concentrations (Fig. S3).

Stocks and fluxes of microbial components

During the late Austral summer, abundances of virus-like particles, heterotrophic bacteria, bacterial production,

Table 4. Bacterial production (BP), Bacterial respiration (BR), cell-specific BP and BR, growth rate (μ) and growth efficiency (BGE) measured at 10 and 60 m. Mean values ± SD for BP, BGE) and ±SE for BR. Bacterial respiration rates have been converted from O_2 into C units using a RQ value of 1. No respiration measurements at M3-1.

Sta.	Depth (m)	BP (nmol C L^{-1} d^{-1})	BR (μmol C L^{-1} d^{-1})	Cell-specific BP (fmol C $cell^{-1}$ d^{-1})	Cell-specific BR (fmol C $cell^{-1}$ d^{-1})	μ (d^{-1})	BGE %
M2-1	10	44.0 ± 0.2	0.68 ± 0.63	0.042	0.64	0.041	6 ± 5
	60	62.0 ± 11.6	2.37 ± 0.24	0.057	2.16	0.055	3 ± 1
M2-2	10	92.5 ± 12.8	0.41 ± 0.29	0.110	0.49	0.107	18 ± 10
	60	71.6 ± 3.2	0.48 ± 0.13	0.090	0.60	0.088	13 ± 3
M2-3	10	113.8 ± 4.0	0.35 ± 0.07	0.157	0.40	0.154	28 ± 4
	60	86.2 ± 1.6	0.35 ± 0.07	0.122	0.45	0.119	21 ± 3
M1	10	43.1 ± 4.0	0.11 ± 0.09	0.078	0.20	0.076	28 ± 16
	60	27.5 ± 2.4	0.11 ± 0.09	0.075	0.22	0.073	25 ± 15
M3-3	10	26.4 ± 2.0	0.29 ± 0.13	0.048	0352	0.046	8 ± 4
	60	27.5 ± 2.4	0.32 ± 0.06	0.057	0.66	0.056	8 ± 2
M4-1	10	28.0 ± 3.6	0.91 ± 0.15	0.040	1.30	0.039	3 ± 1
	60	26.2 ± 2.4	0.41 ± 0.32	0.043	0.67	0.042	6 ± 4
M4-2	10	28.8 ± 4.0	0.22 ± 0.11	0.052	0.39	0.050	12 ± 5
	60	29.6 ± 4.0	0.38 ± 0.15	0.053	0.68	0.052	7 ± 3

heterotrophic nanoflagellates (HNF), and phototrophic pico- and nanophytoplankton were higher on the plateau (Sta. M2) than at the off-plateau stations (M1, M3, and M4, Fig. 3a–e). These differences were more pronounced in the mixed layer and were attenuated at depth. The proportion of "high nucleic acid" bacteria was slightly higher on the plateau (56%) than off the plateau (44%, Table 3). The proportion of the two virus-like particles populations identified based on their fluorescence was similar at all sites, with low fluorescence virus-like particles dominating throughout the water column (84–90%) (Table 3). *Synechococcus* was found at low abundances of a magnitude of 10^4 cells L^{-1} (Table 3). Bacterial production, averaged over the three visits, was about 2-fold higher in the mixed layer at Sta. M2 than the off-plateau stations (Table 3). Bacterial respiration in the mixed layer on the plateau (mean 0.45 ± 0.14 μmol O_2 L^{-1} d^{-1}) was not different to that determined off the plateau (mean 0.38 ± 0.26 μmol O_2 L^{-1} d^{-1}), with the exception of one high value recorded during the first visit of Sta. M2 (Table 4). As a consequence, bacterial growth efficiency was substantially higher on the plateau during the 2nd and 3rd visit (mean $20 \pm 6\%$) than off the plateau at Sta. M3 and M4 (mean $7 \pm 3\%$). Bacterial growth rates were also higher during the 2nd and 3rd visit of Sta. M2 (0.12 ± 0.03 d^{-1}) as compared to the off-plateau stations (0.05 ± 0.00 d^{-1}) (Table 4).

Loss of bacteria due to grazing and viral lysis

As revealed by microscopic observations, HNF and ciliates were ingesting FLB (Fig. S4). Because of their higher abundance when compared to ciliates (0.2–0.5 10^3 ciliates L^{-1}), HNF (10^6 HNF L^{-1}) were the major bacterial grazers. On average, 60% (range 38–87%) of the HNF ingested in most cases 1–3 FLB. The few ciliates observed on the filters contained 5 to > 10 FLB CIL^{-1}. Small dinoflagellate *Gymnodinium* spp. cells of 10–20 μm accounted for 0.7–1.0 10^3 cells L^{-1} (data not shown) and they occasionally contained 1–3 FLB *Gymnodinium* $^{-1}$. Finally, FLB ingestion occurred in less than 1% of nanophytoplankton observed on the filters (cf. Fig. S4). Based on all observations, the ingestion rate was of about 1–3 bact $grazer^{-1}$ h^{-1} (mean 1.4, median 1.3 bact $grazer^{-1}$ h^{-1}, Fig. 4a). The loss of bacterial production induced by grazing was calculated based on the estimated ingestion rate multiplied by the number of grazers. Grazing on bacteria was higher at Sta. M2 (median 105%) than off-plateau stations (median 80%) (Fig. 4b). By contrast, the virus-induced mortality was comparatively low, varying from undetectable values at M2-3 to 15% at M2-2 (median 9% for all stations) (Fig. 4c).

Short-term temporal variability

The higher microbial stocks and fluxes measured on the plateau at Sta. M2 were also accompanied by a more pronounced variability between the three visits as compared to off-plateau waters. Concentrations of Chl *a* and the abundance of pico- and nanophytoplankton in the mixed layer

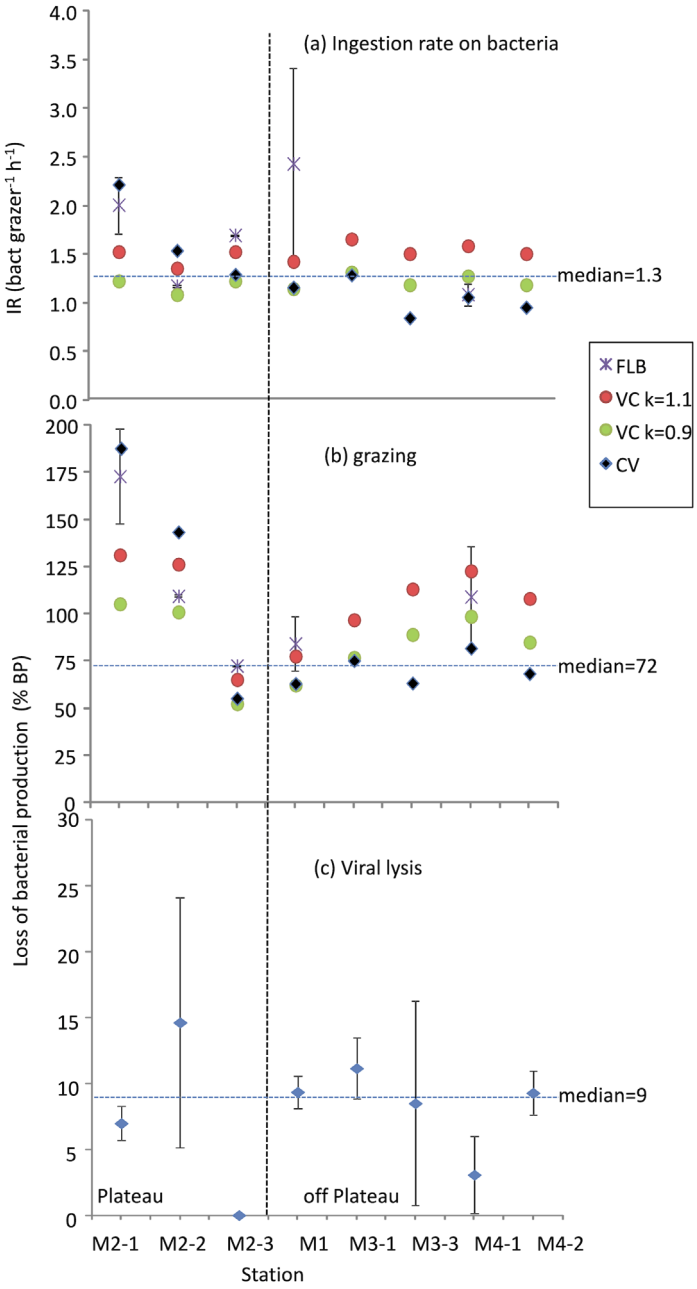

Fig 4. Mean ingestion rates on bacteria (**a**), proportion (%) of bacterial production loss due to grazing (**b**) and proportion (%) of bacterial production loss due to viral lysis (**c**). FLB: based on FLB disappearance, error bars for FLB indicate standard deviation (SD) between replicates. The estimation based on vacuole content (VC) analysis was calculated for digestion times k = 1.1 and k = 0.9. The estimation based on cell volume (CV) was calculated assuming a clearance rate of 10^5 cell volume h^{-1} of grazers (for more details see M&M section). Error bars indicate SD between replicates for grazing and between different depths in the mixed layer for viral lysis.

increased between the first to the third visit by factors of 2.0 and 2.6, respectively. A similar pattern was observed for bacterial production (3-fold increase, Fig. 3e), while the abundance of heterotrophic bacteria decreased by 1.9-fold during this

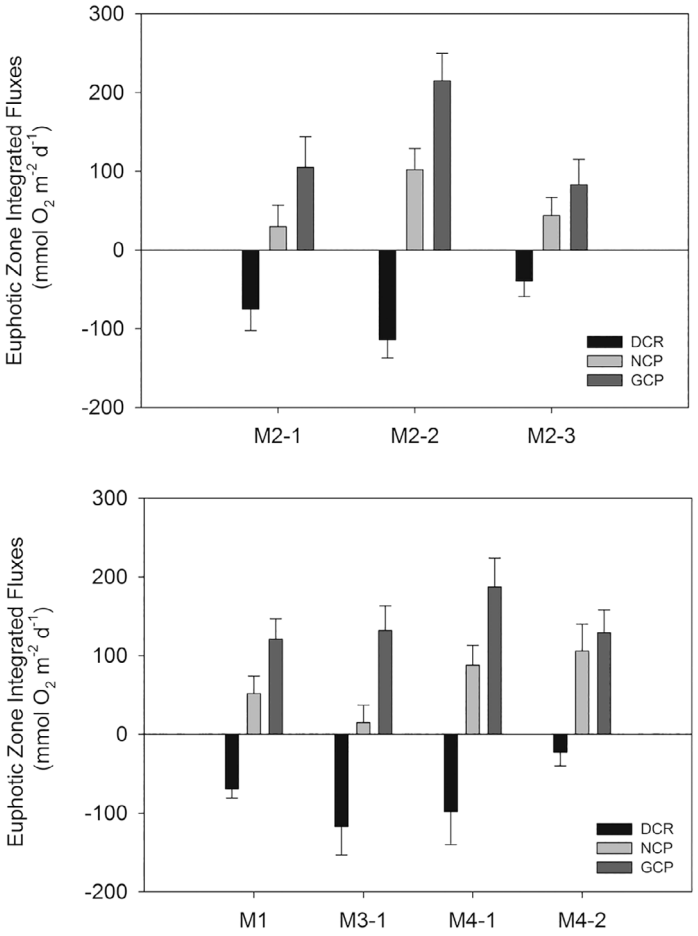

Fig 5. Integrated euphotic layer, gross community production (GCP), dark community respiration (DCR) and net community production (NCP) (mmol O_2 m^{-2} d^{-1}). Error bars represent standard errors.

3-week time period (Fig. 3b). The inverse temporal pattern in bacterial production and heterotrophic bacteria abundance resulted in a 3.7 and 2-fold increase in the bacterial growth rate (μ) and cell-specific bacterial production, respectively (Table 4). Concomitant with the decrease in heterotrophic bacteria abundance, bacterial grazers (HNF) and virus-like particles increased by 2- and 1.5-fold between the first and the second visit of Sta. M2 (Fig. 3a–c). All three bacterivory estimation approaches used in this study revealed higher grazing during the first visit (> 100%) and grazing decreased to 50–75% of the bacterial production during the third visit (Fig. 4b). Off the Kerguelen plateau, the short-term variability was much less pronounced. Noticeable decreases between consecutive visits were observed for the abundance of heterotrophic bacteria and pico- and nanophytoplankton at Sta. M3.

Net community production, dark community respiration, and gross community production

Above the Kerguelen plateau, at Sta. M2, net community production fluxes integrated over the euphotic zone varied between 30 and 44 mmol O_2 m^{-2} d^{-1} during the 1st and 3rd visit. Net community production was substantially higher during the 2nd visit (100 mmol O_2 m^{-2} d^{-1}) (Fig. 5), which could explain the observed increase in the Chl *a* concentrations about 1 week later (Table 1). Off-plateau, highest net community production fluxes were determined at Sta. M4 (88–106 mmol O_2 m^{-2} d^{-1}). Euphotic zone integrated fluxes of dark community respiration varied between 75 and 113 mmol O_2 m^{-2} d^{-1} during the first two visits at Sta. M2 and dark community respiration decreased to 39 mmol O_2 m^{-2} d^{-1} during the 3rd visit. Fluxes of dark community respiration off-plateau ranged between 69 and 117 mmol O_2 m^{-2} d^{-1}, with the exception of the last visit at Sta. M4 (23 mmol O_2 m^{-2} d^{-1}) (Fig. 5), which corresponded to a deepening of the mixed layer following the storm event. Highest depth-integrated fluxes of gross community production were recorded during the 2nd visit at Sta. M2 (215 mmol O_2 m^{-2} d^{-1}) while gross community production ranged between 121 and 187 mmol O_2 m^{-2} d^{-1} off-plateau (Fig. 5). Comparison of the volumetric rates of oxygen consumption in unfiltered and < 0.8 μm filtered seawater revealed that above the Kerguelen plateau bacterial respiration accounted for 41 ± 2% and 87 ± 24% of community respiration at 10 and 60 m, respectively. Off-plateau, bacterial respiration accounted for 100% of community respiration during both visits.

Discussion

Late summer microbial food web

We observed that the microbial standing stocks and fluxes, apart from microbial respiration, were higher in the mixed layer of the iron-fertilized area above the Kerguelen plateau as compared to surrounding HNLC waters, even one month after the decline of the phytoplankton bloom. Our results thereby complement previous observations during the onset and the decline of the Kerguelen bloom (e.g., Table 4 in Christaki et al. 2014). A comparison of the different phases of the bloom reveals, however, distinct features at the end of summer. While the enhancement of Chl *a* and bacterial production on- vs. off-plateau ratios exceeded by 2–4-fold that of the other parameters in early spring and summer, their on- vs. off-plateau ratios were in a similar range during the post bloom period (Table S1, Fig. 6). Pico- and nanophytoplankton were characterized by marked increases in their abundance (about 15-fold) and contribution to total Chl *a* (10–53%) between the onset and the post bloom periods in Kerguelen plateau waters (Table S1). In addition, the ratio of pico- and nanophytoplankton in fertilized vs. HNLC waters was < 1 during the onset and decline of the bloom and > 1 after the bloom (Fig. 6). This observation is in line with previous studies in the Kerguelen area indicating that pico- and nanophytoplankton dominate communities on the plateau before (Christaki et al. 2014) and after the bloom (Uitz

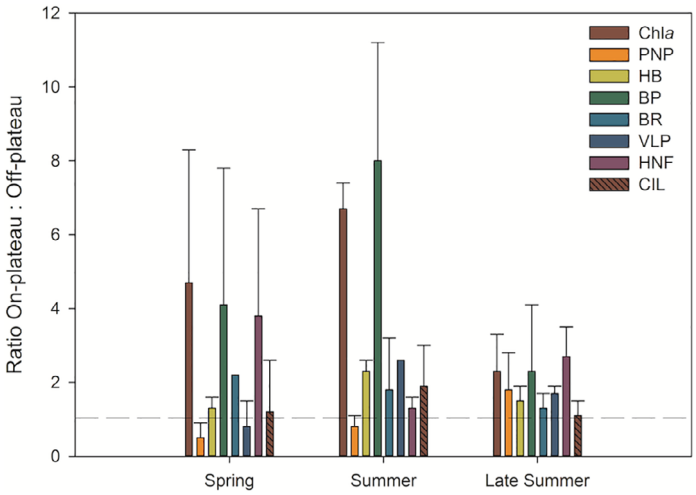

Fig 6. On- vs. off-plateau ratios of microbial parameters in the mixed layer. Chlorophyll *a* (Chl *a*), heterotrophic bacteria (HB), phototrophic pico- and nanoplankton (PNP), bacterial production (BP), bacterial respiration (BR), virus like particles (VLP), heterotrophic nanoflagellates (HNF), and ciliates (CIL).

et al. 2010). Furthermore, estimates of mean annual primary production reveal that pico- and nanophytoplankton (2.5 Gt C yr^{-1}) have a higher contribution as compared to microphytoplankton (0.9 Gt C yr^{-1}, Uitz et al. (2010), underlying their importance in Southern Ocean waters.

Heterotrophic bacteria reached 1.0×10^9 cells L^{-1} during the post bloom period, and their biomass was about 2 to 3-fold higher as compared to those recorded at this station during the onset and decline of the bloom (Table S1). The most important heterotrophic bacterial mortality factors HNF and virus-like particles revealed opposite seasonal trends. While HNF had higher on-/off-plateau ratios during early spring and late summer, virus-like particles revealed highest on-/off-plateau differences in summer (Fig. 6). These observations are coherent with estimates of grazing and viral lysis of heterotrophic bacteria. Grazing was identified as the dominant loss process of heterotrophic bacteria during late summer, and a similar scenario has been observed in early spring (Christaki et al. 2014). The intense bacterial grazing seemed to co-occur with the NH_4 increase between the first and the second visit at Sta. M2 (Table 1, Figs. 4, S3). The methods assessing grazing are based on several assumptions. In the present study, we used three experimental and theoretical approaches to better frame the lower and upper limits of bacterial mortality attributed to grazing. The grazing estimations based on volume specific clearance rates (Fenchel 1982) or digestion times (Dolan and Šimek 1998) were determined in cultures, and even though they are not a direct measure of grazing, they provide representative patterns of the potential of HNF to ingest bacteria. At Sta. M2-1, the obtained values from the different approaches showed the highest variability, however, all values had a consistent pattern in that grazing exceeded bacterial production (Sta. M2-1, CV 26%, Fig. 4). The mean ingestion rates obtained by all methods (1–3 bact. $grazer^{-1}$ h^{-1}) varied within a narrow range, being consistent at all stations and similar to previous observations (e.g., Christaki et al. 2008, 2014; Gast et al. 2018). This mean ingestion rate corresponds to the ingesting capacity of HNF since they were one order of magnitude more abundant than ciliates and *Gymnodinium* spp. despite the higher number of cells they ingest. Few studies have considered grazing by protists and viral mortality simultaneously, particularly in the Southern Ocean (Guixa-Boixereu et al. 2002; Malits et al. 2014; Vaqué et al. 2017). Prey consumption by grazers is expected to be more important than viral activity during early stages of phytoplankton blooms, which could explain the delay between bacterial production and the increase in abundances (Brum et al. 2016). Confirming this hypothesis, in our study, predation was the dominant cause of bacterial mortality during the onset and after the bloom, while viral lysis dominated during the decline of the bloom. During summer (decline of the bloom), virus induced mortality accounted on average 72 ± 72 and 27 ± 19% of bacterial production inside and outside the bloom, respectively. Lysogenic infected bacteria could be detected only in 7 out of 15 essays and ranged from 0 to 31% of infected bacteria on the plateau and from 0 to 4% in HNLC waters, without any significant difference between the two areas (Malits et al. 2014). In the Southern Ocean, a number of studies taking into account viral infection have found consistent high viral lytic production (e.g., Guixa-Boixereu et al. 2002; Evans and Brussaard 2012; Vaqué et al. 2017 and references therein) while lysogeny was varying greatly (e.g., Evans and Brussaard 2012; Vaqué et al. 2017).

Mixotrophy of unicellular eukaryotes is widespread (e.g., Zubkov and Tarran 2008; Stoecker et al. 2017), including in the Southern Ocean (Moorthi et al. 2009; Gast et al. 2018), but the possible triggering factors such as light or nutrient limitation remain largely unresolved. Even though pico- and nanophytoplankton were abundant at all stations during MOBYDICK, we observed insignificant uptake of FLB by nanophytoplankton. It was therefore impossible to evaluate accurately mixotrophic activity in the present study. In oligotrophic systems, pico- and nanophytoplankton can account for up to 95% of bacterivory (Zubkov and Tarran 2008). In this case, phagocytosis might be advantageous to photosynthetic organisms as it provides an increased access to limiting nutrients. This could suggest that the nutrient and light conditions were optimal for pico- and nanophytoplankton growth during late summer in the Kerguelen region, and phototrophic cells did not need to complement their diet by ingesting bacteria. However, in a study in the eastern Mediterranean (Christaki et al. 1999) it was found that 12% of nanophytoplankton ingested small spherical FLB called "minicells" (*E. coli* X-1488, 0.65 μm in diameter), while only 6% ingested larger elongated

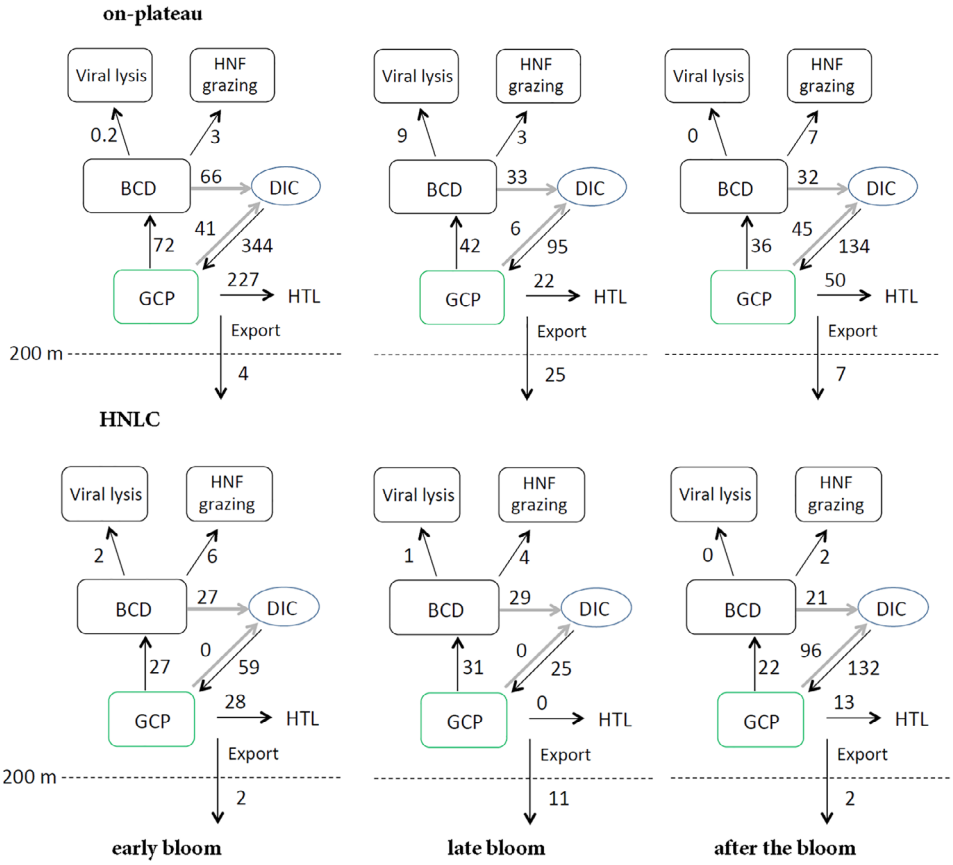

Fig 7. Mixed layer integrated carbon flow within the microbial food web. From left to right: during early (KEOPS2), late (KEOPS1), and after the diatom bloom (MOBYDICK). KEOPS2 and KEOPS1 on-plateau stations were redrawn from Christaki et al. 2014 (and references therein). Values from MOBYDICK refer to the mean of the three visits at M2. All fluxes are integrated in the mixed layer and units are mmol C m^{-2} d^{-1}. Arrows in gray indicate rates of bacterial respiration (BR) and dark community respiration (DCR). Bacterial carbon demand (BCD) defined as BCD = bacterial production (BP) + bacterial respiration (BR), dissolved inorganic carbon (DIC), gross community production (GCP), biomass available for higher trophic levels (HTL), defined as HTL = GCP-(DCR+BCD+export). MOBYDICK export data were calculated based on the ^{234}Th approach (Planchon pers. comm., the method is described in detail in Planchon et al. 2015). Late bloom (KEOPS1) data from Carlotti et al. (2008), Christaki et al. (2008), Lefèvre et al. (2008), Obernosterer et al. (2008), Savoye et al. (2008) and Malits et al. (2014). Early bloom data (KEOPS 2) from Planchon et al. (2015) and Carlotti et al. (2015), Christaki et al. (2014).

FLB (approx. 0.8 μm ESD: equivalent spherical diameter) as the ones used here (Fig. S4). Thus, selection against the FLB is also a possibility and it most likely depends on the prevailing taxonomic groups. During MOBYDICK, nanophytoplankton were dominated at all stations by the prymnesiophyte *Phaeocystis antarctica* (> 70% based on pigment and microscopic data; Irion et al. 2020), which is known to be widespread in the Southern Ocean (Poulton et al. 2007; Gast et al. 2018). Contrary to many prymnesiophytes, mixotrophic activity has not been reported so far for *P. antarctica* (Gast et al. 2018). We therefore suggest one of the following possibilities, or a combination of them, to explain our results on mixotrophy: (i) a selection against the FLB used in this study; (ii) environmental conditions leading to low bacterivory by phototrophs; and (iii) the dominance of non-mixotrophic cells such as *P. antarctica*.

Seasonal microbial dynamics and ecosystem functioning

Combining the observations made during late summer (MOBYDICK project) with those from previous projects carried out in early spring (KEOPS2) and summer (KEOPS1) has allowed us to draw a seasonal scenario for microbial food web fluxes in iron-fertilized and HNLC waters. In Kerguelen plateau waters, the three observation periods corresponded to the onset, decline, and post phytoplankton bloom phase (Fig. 7, Table 5). In early spring, the system is highly productive, with low carbon export and carbon export efficiency, resulting in a large amount of phytoplankton carbon potentially available for higher trophic levels. During the decline of the bloom, gross community production decreases by 3-fold as compared to early spring. The system is characterized by high carbon export and carbon export efficiency while phytoplankton carbon potentially available for higher trophic levels is 10-fold

Table 5. Seasonal ecosystem characteristics and microbial food web dynamics above the Fe-fertilized Kerguelen plateau and in HNLC waters. Productivity regime refers to gross community production (GCP), export efficiency is the ratio of carbon exported below 200 m to GCP, bacterial growth efficiency (BGE), heterotrophic nanoflagellates (HNF). Early spring and summer BGE and microbial food web fluxes from Lefèvre et al. 2008; Obernosterer et al. 2008, Christaki et al. 2014; Malits et al. 2014 (see also Fig. 7).

	Productivity regime	Export efficiency	Biomass available for higher trophic levels	Microbial food web fluxes (MFW)
Kerguelen plateau				
Early spring: Onset of the bloom	High (344)	Low (1%)	High (227)	Moderate fraction of C channeled through MFW (21%) Low BGE (9%) Transfer to HNF (50%) dominates over viral lysis (3%)
Summer: Decline of the bloom	Moderate (95)	High (26%)	Low (22)	High fraction of C channeled through MFW (44%) High BGE (18%) Viral lysis dominates (>80%) over HNF (34%)
Late summer: Post bloom	Moderate (134)	Low (4%)	Moderate (50)	Moderate fraction of C channeled through MFW (27%) High BGE (17%) Transfer to HNF dominates (76%) over viral lysis (7%)
HNLC waters				
Early spring	Moderate (59)	Low (3%)	Moderate (30)	High fraction of C channeled through MFW (46%) Low BGE (3%) Transfer to HNF (69%) dominates over viral lysis (20%)
Summer	Low (25)	High (44%)	Low (0)	High fraction of C channeled through MFW (100%) Low BGE (8%) Transfer to HNF (95%) dominates over viral lysis (10%)
Late summer	Moderate (132)	Low (2%)	Low (12)	Moderate fraction of C channeled through MFW (17%) Low BGE (8%) Transfer to HNF (97%) dominates over viral lysis (11%)

lower as compared to spring. During the post-bloom phase, gross community production is similar to that determined during the declining bloom phase. However, carbon export and export efficiency are again low, resulting in biomass available for higher trophic levels roughly 2-fold higher as compared to the bloom decline (Fig. 7, Table 5).

Heterotrophic bacteria contribute substantially to carbon processing during all stages. The fraction of total biomass available for higher trophic levels accounted for by bacteria is minor during early spring (< 1%) and it increases up to 14% during the declining and post-bloom phases (Fig. 7, Table 5). In addition, bacteria have a substantial contribution to microbial community respiration (42% and 85% of dark community respiration). The role of the microbial food web for carbon processing varies during the three stages (Table 5). In early spring, a moderate fraction of primary production is channeled through bacteria (21%) and due to a low bacterial growth efficiency (9%) this organic matter is mainly respired. During the decline of the bloom, heterotrophic bacteria process a higher fraction of primary production (44%) with a more efficient bacterial biomass production as compared to spring (bacterial growth efficiency of 18%, Table S1). The importance of viral lysis in carbon losses results in an inefficient transfer of bacterial biomass to HNF. During the post bloom phase, organic carbon is processed with a bacterial growth efficiency (17%) similar to the declining bloom phase, and the transfer to HNF dominates over the loss by viral lysis. Taken together, these observations suggest an overall less efficient microbial food web during early spring and summer with respiration and viral lysis, respectively, representing important loss terms. During the post bloom period, roughly 30% of the gross community production are efficiently transferred to bacterial biomass and HNF, suggesting a good functioning of the microbial loop.

In HNLC waters, a seasonal pattern similar to that in iron-fertilized waters can be depicted, though with fluxes that are less variable among periods (Fig. 7, Table 5). In contrast to iron-fertilized waters, most of the gross community production is remineralized, leading to lower export and biomass available for higher trophic levels. Heterotrophic bacteria dominate microbial community respiration in early spring and summer, and their contribution decreases to 18% at the end of the season. Similarly, bacteria process large fractions of primary production in early spring (45%) and in summer (100%), and this fraction substantially decreases in late summer (17%). Despite the low bacterial growth efficiency (3–8%), the carbon processed by bacteria supports the microbial food web as grazing by HNF dominates over viral lysis. These

observations illustrate the quantitative importance of microbial food web processes across seasons and productivity regimes in the Southern Ocean.

What are the potential consequences of climate-driven environmental changes on the role of microbes in food webs of cold-water environments? The Southern Ocean is a major storage reservoir of heat, thus the warming of surface waters is expected to affect microbial communities (Morán et al. 2010; Kim and Ducklow 2016). Temperature and the supply of bioavailable dissolved organic matter were identified as key factors for bacterial biomass and growth in polar waters (Kirchman et al. 2009). Warming is expected to increase total and dissolved phytoplankton primary production (Morán et al. 2006; Boyd et al. 2016; Deppeler and Davidson 2017), which could result in a stronger coupling to bacteria through the utilization of dissolved organic matter (Vaqué et al. 2019). These observations suggest an increasingly important role of heterotrophic bacteria. In this context, our data provide two interesting observations. Firstly, the high contribution of bacteria to community respiration, and secondly the amount of carbon transferred in the form of bacterial biomass to HNF, which is in the same range as the carbon export (2–7 mmol C m^{-2} d^{-1}) in early spring and late summer. Thus, the predicted changes could lead to an increase in the amount of phytoplankton-derived organic matter consumed by bacteria. Temperature effects on the bacterial growth efficiency are uncertain (López-Urrutia and Morán 2007), leaving the question on the quantitative importance of organic carbon remineralization open (Sarmento et al. 2010). The increased flow of carbon to bacterial biomass and HNF could support higher trophic levels, but in turn lead to a weakening of the Southern Ocean capacity to sequester organic carbon.

References

Binder, B. 1999. Reconsidering the relationship between virally induced bacterial mortality and frequency of infected cells. Aquat. Microb. Ecol. **18**: 207–215. doi:10.3354/ame018207

Blain, S., et al. 2007. Effect of natural iron fertilization on carbon sequestration in the Southern Ocean. Nature **446**: 1070–1074. doi:10.1038/nature05700

Boyd, P. W., and others. 2016. Physiological responses of a Southern Ocean diatom to complex future ocean conditions. Nat. Clim. Change **6**: 207–213. doi:10.1038/nclimate2811

Brum, J. R., B. L. Hurwitz, O. Schofield, H. W. Ducklow, and M. B. Sullivan. 2016. Seasonal time bombs: dominant temperate viruses affect Southern Ocean microbial dynamics. ISME J. **10**: 437–449. doi:10.1038/ismej.2015.125

Brussaard, C. P. D. 2004. Optimization of procedures for counting viruses by flow cytometry. Appl. Environ. Microbiol. **70**: 1506–1513. doi:10.1128/AEM.70.3.1506-1513.2004

Carlotti, F., et al. 2015. Mesozooplankton structure and functioning during the onset of the Kerguelen phytoplankton bloom during the KEOPS2 survey. Biogeosciences **12**: 4543–4563. doi:10.5194/bg-12-4543-2015

Carlotti, F., D., Thibault-Botha, A. Nowaczyk, and D. Lefèvre. 2008. Zooplankton community structure, biomass and role in carbon fluxes during the second half of a phytoplankton bloom in the eastern sector of the Kerguelen Shelf (January–February 2005). Deep Sea Research Part II: Topical Studies in Oceanography **55**: 720–733. doi:10.1016/j.dsr2.2007.12.010

Cavagna, A. J., and others. 2015. Production regime and associated N cycling in the vicinity of Kerguelen Island, Southern Ocean. Biogeosciences **12**: 6515–6528. doi:10.5194/bg-12-6515-2015

Christaki, U., F. Van Wambeke, and J. Dolan. 1999. Nanoflagellates (mixotrophs, heterotrophs and autotrophs) in the oligotrophic eastern Mediterranean:standing stocks, bacterivory and relationships with bacterial production. Mar. Ecol. Prog. Ser. **181**: 297–307. doi:10.3354/meps181297

Christaki, U., I. Obernosterer, F. Van Wambeke, M. Veldhuis, N. Garcia, and P. Catala. 2008. Microbial food web structure in a naturally iron-fertilized area in the Southern Ocean (Kerguelen Plateau). Deep Sea Res. Part II: Top. Stud. Oceanogr. **55**: 706–719. doi:10.1016/j.dsr2.2007.12.009

Christaki, U., C. Courties, R. Massana, P. Catala, P. Lebaron, J. M. Gasol, and M. V. Zubkov. 2011. Optimized routine flow cytometric enumeration of heterotrophic flagellates using SYBR Green I: FC analysis of HF. Limnol. Oceanogr.: Methods **9**: 329–339. doi:10.4319/lom.2011.9.329

Christaki, U., and others. 2014. Microbial food web dynamics during spring phytoplankton blooms in the naturally iron-fertilized Kerguelen area (Southern Ocean). Biogeosciences **11**: 6739–6753. doi:10.5194/bg-11-6739-2014

Deppeler, S. L., and A. T. Davidson. 2017. Southern Ocean phytoplankton in a changing climate. Front. Mar. Sci. **4**: 40. doi:10.3389/fmars.2017.00040

Dolan, J. R., and K. Šimek. 1998. Ingestion and digestion of an autotrophic picoplankter, Synechococcus, by a heterotrophic nanoflagellate, Bode saLtans. Limnol. Oceanogr. **43**: 1740–1746. doi:10.4319/lo.1998.43.7.1740

Evans, C., and C. P. D. Brussaard. 2012. Regional variation in lytic and lysogenic viral infection in the Southern Ocean and its contribution to biogeochemical cycling. Appl. Environ. Microbiol. **78**: 6741–6748. doi:10.1128/AEM.01388-12

Fenchel, T. 1982. Ecology of heterotrophic microflagellates. IV: Quantitative occurrence and importance as bacterial consumers. Mar. Ecol. Prog. Ser. **9**: 35–42. doi:10.3354/meps009035

Gast, R. J., S. A. Fay, and R. W. Sanders. 2018. Mixotrophic activity and diversity of antarctic marine protists in austral summer. Front. Mar. Sci. **5**: 13. doi:10.3389/fmars.2018.00013

Gray, A. R., and others. 2018. Autonomous biogeochemical floats detect significant carbon dioxide outgassing in the high-latitude Southern Ocean. Geophys. Res. Lett. **45**: 9049–9057. doi:10.1029/2018GL078013

Gruber, N., et al. 2009. Oceanic sources, sinks, and transport of atmospheric CO_2: Oceanic sources, sinks and transport of CO_2. Global Biogeochem. Cycles **23**. doi:10.1029/2008GB003349

Guixa-Boixereu, N., D. Vaqué, J. M. Gasol, J. Sánchez-Cámara, and C. Pedrós-Alió. 2002. Viral distribution and activity in Antarctic waters. Deep-Sea Res. Part II: Top. Stud. Oceanogr. **49**: 827–845. doi:10.1016/S0967-0645(01)00126-6

Irion, S., L. Jardillier, I. Sassenhagen, and U. Christaki. 2020. Marked spatio-temporal variations in small phytoplankton structure in contrasted waters of the Southern Ocean (Kerguelen area). Limnol. Oceanogr. **9999**: 1–18. doi:10.1002/lno.11555

Kim, H., and H. W. Ducklow. 2016. A decadal (2002–2014) analysis for dynamics of heterotrophic bacteria in an Antarctic coastal ecosystem: Variability and physical and biogeochemical forcings. Front. Mar. Sci. **3**: 214. doi:10.3389/fmars.2016.00214

Kirchman, D. L. 1993. Leucine incorporation as a measure of biomass production by heterotrophic bacteria, p. 509–512. *In* P. F. Kemp, B. F. Sherr, E. B. Sherr, and J. J. Cole [eds.], Handbook of methods in aquatic microbial ecology. Boca Raton, FL: Lewis Publishers.

Kirchman, D. L., X. A. G. Morán, and H. Ducklow. 2009. Microbial growth in the polar oceans—role of temperature and potential impact of climate change. Nat. Rev. Microbiol. **7**: 451–459. doi:10.1038/nrmicro2115

Lam, P. J., and J. K. B. Bishop. 2007. High biomass, low export regimes in the Southern Ocean. Deep-Sea Res. Part II: Top. Stud. Oceanogr. **54**: 601–638. doi:10.1016/j.dsr2.2007.01.013

Lasbleiz, M., K. Leblanc, L. K. Armand, U. Christaki, C. Georges, I. Obernosterer, and B. Quéguiner. 2016. Composition of diatom communities and their contribution to plankton biomass in the naturally iron-fertilized region of Kerguelen in the Southern Ocean. FEMS Microbiol. Ecol. **92**: fiw171. doi:10.1093/femsec/fiw171

Lê, S., J. Josse, and F. Husson. 2008. FactoMineR: An R package for multivariate analysis. J. Stat. Softw. **25**: 1–18.

Lefèvre, D., C. Guigue, and I. Obernosterer. 2008. The metabolic balance at two contrasting sites in the Southern Ocean: The iron-fertilized Kerguelen area and HNLC waters. Deep-Sea Res. Part II: Top. Stud. Oceanogr. **55**: 766–776. doi:10.1016/j.dsr2.2007.12.006

LeMoigne, F. A. C., et al. 2016. What causes the inverse relationship between primary production and export efficiency in the Southern Ocean? Geophys. Res. Lett. **43**: 4457–4466. doi:10.1002/2016GL068480

López-Urrutia, Á., and X. A. G. Morán. 2007. Resource limitation of bacterial production distorts the temperature dependence of oceanic carbon cycling. Ecology **88**: 817–822.

Maiti, K., M. A. Charette, K. O. Buesseler, and M. Kahru. 2013. An inverse relationship between production and export efficiency in the Southern Ocean. Geophys. Res. Lett. **40**: 1557–1561. doi:10.1002/grl.50219

Malits, A., U. Christaki, I. Obernosterer, and M. G. Weinbauer. 2014. Enhanced viral production and virus-mediated mortality of bacterioplankton in a natural iron-fertilized bloom event above the Kerguelen Plateau. Biogeosciences **11**: 6841–6853. doi:10.5194/bg-11-6841-2014

Moorthi, S., D. Caron, R. Gast, and R. Sanders. 2009. Mixotrophy: a widespread and important ecological strategy for planktonic and sea-ice nanoflagellates in the Ross Sea, Antarctica. Aquat. Microb. Ecol. **54**: 269–277. doi:10.3354/ame01276

Morán, X. A. G., M. Sebastián, C. Pedrís-Alií, and M. Estrada. 2006. Response of Southern Ocean phytoplankton and bacterioplankton production to short-term experimental warming. Limnol. Oceanogr. **51**: 1791–1800. doi:10.4319/lo.2006.51.4.1791

Morán, X. A. G., Á. López-Urrutia, A. Calvo-Díaz, and W. K. W. Li. 2010. Increasing importance of small phytoplankton in a warmer ocean. Glob. Change Biol. **16**: 1137–1144. doi:10.1111/j.1365-2486.2009.01960.x

Mosseri, J., B. Quéguiner, L. Armand, and V. Cornet-Barthaux. 2008. Impact of iron on silicon utilization by diatoms in the Southern Ocean: A case study of Si/N cycle decoupling in a naturally iron-enriched area. Deep-Sea Res. Part II: Top. Stud. Oceanogr. **55**: 801–819. doi:10.1016/j.dsr2.2007.12.003

Obernosterer, I., U. Christaki, D. Lefèvre, P. Catala, F. Van Wambeke, and P. Lebaron. 2008. Rapid bacterial mineralization of organic carbon produced during a phytoplankton bloom induced by natural iron fertilization in the Southern Ocean. Deep-Sea Res. Part II: Top. Stud. Oceanogr. **55**: 777–789. doi:10.1016/j.dsr2.2007.12.005

Oksanen, J. and others. 2017. vegan: Community Ecology Package. R package version 2.3-0. 2015.

Pauthenet, E., F. Roquet, G. Madec, C. Guinet, M. Hindell, C. R. McMahon, R. Harcourt, and D. Nerini. 2018. Seasonal Meandering of the Polar front upstream of the Kerguelen plateau. Geophys. Res. Lett. **45**: 9774–9781. doi:10.1029/2018GL079614

Planchon, F., and others. 2015. Carbon export in the naturally iron-fertilized Kerguelen area of the Southern Ocean based on the ^{234}Th approach. Biogeosciences **12**: 3831–3848. doi:10.5194/bg-12-3831-2015

Pollard, R., R. Sanders, M. Lucas, and P. Statham. 2007. The Crozet natural iron bloom and export experiment (CROZEX). Deep-Sea Res. Part II: Top. Stud. Oceanogr. **54**: 1905–1914. doi:10.1016/j.dsr2.2007.07.023

Pollard, R. T., and others. 2009. Southern Ocean deep-water carbon export enhanced by natural iron fertilization. Nature **457**: 577–580. doi:10.1038/nature07716

Poulton, A. J., C. Mark Moore, S. Seeyave, M. I. Lucas, S. Fielding, and P. Ward. 2007. Phytoplankton community composition around the Crozet Plateau, with emphasis on diatoms and Phaeocystis. Deep-Sea Res. Part II: Top. Stud. Oceanogr. **54**: 2085–2105. doi:10.1016/j.dsr2.2007.06.005

Rembauville, M., S. Blain, L. Armand, B. Quéguiner, and I. Salter. 2015. Export fluxes in a naturally iron-fertilized area of the Southern Ocean—Part 2: Importance of diatom resting spores and faecal pellets for export. Biogeosciences **12**: 3171–3195. doi:10.5194/bg-12-3171-2015

Sarmento, H., J. M. Montoya, E. Vázquez-Domínguez, D. Vaqué, and J. M. Gasol. 2010. Warming effects on marine microbial food web processes: How far can we go when it comes to predictions? Philos. Trans. R. Soc. B **365**: 2137–2149. doi:10.1098/rstb.2010.0045

Savoye, N., T. W. Trull, S. H. M. Jacquet, J. Navez, and F. Dehairs. 2008. ^{234}Th-based export fluxes during a natural iron fertilization experiment in the Southern Ocean (KEOPS). Deep-Sea Res. Part II: Top. Stud. Oceanogr. **55**: 841–855. doi:10.1016/j.dsr2.2007.12.036

Seeyave, S., M. I. Lucas, C. M. Moore, and A. J. Poulton. 2007. Phytoplankton productivity and community structure in the vicinity of the Crozet Plateau during austral summer 2004/2005. Deep-Sea Res. Part II: Top. Stud. Oceanogr. **54**: 2020–2044. doi:10.1016/j.dsr2.2007.06.010

Sherr, B. F., E. B. Sherr, and R. D. Fallon. 1987. Use of monodispersed, fluorescently labeled bacteria to estimate in situ protozoan bacterivoryt. Appl. Environ. Microbiol. **53**: 8.

Stoecker, D. K., P. J. Hansen, D. A. Caron, and A. Mitra. 2017. Mixotrophy in the marine plankton. Annu. Rev. Mar. Sci. **9**: 311–335. doi:10.1146/annurev-marine-010816-060617

Strzepek, R. F., M. T. Maldonado, J. L. Higgins, J. Hall, K. Safi, S. W. Wilhelm, and P. W. Boyd. 2005. Spinning the "Ferrous Wheel": The importance of the microbial community in an iron budget during the FeCycle experiment: MIcrobial Iron Recycling. Glob. Biogeochem. Cycles **19**. doi:10.1029/2005GB002490

Uitz, J., H. Claustre, B. Gentili, and D. Stramski. 2010. Phytoplankton class-specific primary production in the world's oceans: Seasonal and interannual variability from satellite observations: Phytoplankton class-specific production. Glob. Biogeochem. Cycles **24**. doi:10.1029/2009GB003680

Vaqué, D., et al. 2017. Viruses and protists induced-mortality of prokaryotes around the Antarctic Peninsula during the Austral summer. Front. Microbiol. **8**: 214. doi:10.3389/fmicb.2017.00241

Vaqué, D., and others. 2019. Warming and CO_2 enhance arctic heterotrophic microbial activity. Front. Microbiol. **10**: 494. doi:10.3389/fmicb.2019.00494

Weinbauer, M., C. Winter, and M. Höfle. 2002. Reconsidering transmission electron microscopy based estimates of viral infection of bacterioplankton using conversion factors derived from natural communities. Aquat. Microb. Ecol. **27**: 103–110. doi:10.3354/ame027103

Zubkov, M. V., and G. A. Tarran. 2008. High bacterivory by the smallest phytoplankton in the North Atlantic Ocean. Nature **455**: 224–226. doi:10.1038/nature07236

Acknowledgments

We thank B. Quéguiner, the PI of the MOBYDICK project, for providing us the opportunity to participate to this cruise, the captain and crew of the R/V Marion Dufresne for their enthusiasm and support aboard during the MOBYDICK–THEMISTO cruise (https://doi.org/10.17600/18000403) and the chief scientist I. Obernosterer. This work was supported by the French oceanographic fleet ("Flotte océanographique française"), the French ANR ("Agence Nationale de la Recherche", AAPG 2017 program, MOBYDICK Project number: ANR-17-CE01-0013), and the French Research program of INSU-CNRS LEFE/CYBER ("Les enveloppes fluides et l'environnement"—"Cycles biogéochimiques, environnement et ressources"). This work was also supported by ULCO (Université du Littoral) and CPER MARCO (https://marco.univ-littoral.fr/). We thank three anonymous reviewers and the editors for their comments which helped to improve this work.

Conflict of Interest

None declared.

Submitted 20 March 2020
Revised 03 June 2020
Accepted 16 July 2020

Associate editor: Leila Hamdan